Materials Science and Engineering C 46 (2015) 158–165

Contents lists available at ScienceDirect

Materials Science and Engineering C

journal homepage: www.elsevier.com/locate/msec

Environmental pH-controlled loading and release of protein on mesoporous hydroxyapatite nanoparticles for bone tissue engineering

Ning Zhang [a,b], Tianlin Gao [c], Yu Wang [b], Zongliang Wang [a], Peibiao Zhang [b,*], Jianguo Liu [a,*]

[a] Department of Orthopaedic Surgery, The First Hospital of Jilin University, Xinmin Street No. 71, Changchun TX: 130021, PR China
[b] Key Laboratory of Polymer Ecomaterials, Changchun Institute of Applied Chemistry, Chinese Academy of Sciences, Changchun TX: 130022, PR China
[c] School of Public Health, Jilin University, Changchun 130021, PR China

ARTICLE INFO

Article history:
Received 12 May 2014
Received in revised form 3 September 2014
Accepted 2 October 2014
Available online 5 October 2014

Keywords:
Hydroxyapatite
Mesostructure
Protein delivery
Controlled release
pH value

ABSTRACT

To explore the controlled delivery of protein drugs in micro-environment established by osteoblasts or osteoclasts, the loading/release properties of bovine serum albumin (BSA) depending on pH environment were assessed. The adsorption amounts over mesoporous hydroxyapatite (MHA) or hydroxyapatite (HA) decreased as the pH increased, negatively correlating with zeta-potential values. The adsorption behavior over MHA fits well with the Freundlich and Langmuir models at different pHs. The results suggest that the adsorbed amount of protein on MHA or HA depended on the pH of protein solution. MHA adsorbed BSA at basic pH ($MHA_{pH\ 8.4}$) exhibited a different release kinetics compared with those in acid and neutral environments ($MHA_{pH\ 4.7}$ and $MHA_{pH\ 7.4}$), indicating that the release of protein could be regulated by environmental pH at which MHAs adsorb protein. $MHA_{pH\ 8.4}$ showed a sustained release for 6 h before a gradual release when immersing in acidic environment, which is 2 h longer than that in neutral environment. This suggests that $MHA_{pH\ 8.4}$ showed a more sustained release in acidic environment, which can be established by osteoclasts. The variation of adsorption strength between protein and MHA may be responsible for these behaviors. Our findings may be very useful for the development of MHA applications on both bone repair and protein delivery.

1. Introduction

During the past decade, lots of effort have been made to develop novel drug storage/release systems which exhibit numerous advantages over the conventional forms of dosage, such as enhanced bioavailability, greater efficacy and safety, controlled and prolonged release over time, and predictable therapeutic response [1–8]. In general, an efficient delivery system should be able to deliver the desired drug molecules or bioactive protein to the targeted cells or tissues, and release it in a controlled manner [9]. Nano-scale materials are coming into prominence as a new generation of drug carriers [6,10–12]. For instance, nano-particles can be modified to target and deliver therapeutic agents to treat disease, since drugs delivered via a carrier can help overcome problems inherent in systemic treatment [1,2,13].

Hydroxyapatite particles [HA, $Ca_{10}(PO_4)_6(OH)_2$)] with various morphologies and surface properties have been investigated as protein delivery device due to their biocompatible, nontoxic, and noninflammatory properties [11,14–17]. Protein loading on HA is carried out by surface physical adsorption. However, the adsorption capacity of HA, which mainly depends on the surface area, is limited. Moreover, protein release kinetics showed burst behavior due to weak bonds between protein and HA. Recently, ordered mesoporous hydroxyapatite (MHA) particles have been synthesized and regarded as excellent candidates for protein delivery due to properties such as high surface areas, small and tunable pore sizes, and large pore volumes [18–20], all of which are benefits for effective loading and sustained release of proteins [9,10,21].

The adsorption behaviors of large biomolecules onto hydroxyapatite have been frequently studied [16,17,19,22]. To our knowledge, attention has been focused on the amount of adsorption for large biomolecules, while models of adsorption onto MHA have scarcely been mentioned in the previous papers. Wassell et al. found that biomolecule adsorption behavior on traditional hydroxyapatite particles fitted with the Langmuir model [23], and Lee et al. drew a conclusion that bovine serum albumin (BSA) and lysozyme adsorption onto amino acid-functionalized hydroxyapatite particles fitted better into the Freundlich model than the Langmuir model [22]. However, whether biomolecule adsorption on MHA exhibits similar behavior has not been reported. It is thus worthwhile to investigate the biomolecule adsorption behavior of MHA as this material may play an increasingly important role as a delivery device.

Mesoporous material loading of bioactive proteins has been used for bone repair in recent years [19,21,24–29] where the complicated micro-environment of the human body has to be considered for MHA,

* Corresponding authors.
E-mail addresses: zhangpb@ciac.ac.cn (P. Zhang), jgliu2005@yahoo.com.cn (J. Liu).

http://dx.doi.org/10.1016/j.msec.2014.10.014
0928-4931/

especially different pH values. The pH of the normal extracellular fluid is about 7.4, while the osteoclast establishes an acidic micro-environment between itself and the bone wherein matrix degradation occurs by a process involving proton transport [30]. The local pH around the ruffled border of osteoclasts is from 4.0 to 5.0 [31,32]. Osteoprotegerin (OPG), which belongs to the tumor necrosis factor (TNF) receptor superfamily [33], is known to negatively regulate osteoclast maturation and activation and to promote apoptosis [33–35]. Realizing the controlled release of OPG under acid conditions is very promising. Wassell et al. have demonstrated that the strength of interactions between protein and particle surfaces varies with pH [23]. Therefore we assume that MHA adsorbed protein may show different release patterns in acidic and neutral environments. What is expected is that controlled release may be obtained through control of environmental pH for adsorption or release (Scheme 1).

We report here the successful synthesis of MHA using cationic surfactant as the template. We further described the adsorption behavior of BSA over HA and MHA at different pH values and the release behavior from MHA in acidic and neutral environments. BSA was chosen as the model protein based on its comparatively large dimensions ($40 \times 40 \times 140$ Å^3).

2. Experimental section

2.1. Materials

Cetyltrimethylammonium bromide (CTAB) was purchased from Shanghai Huishi Chemical Co., Ltd., and $(NH_4)_2HPO_4$, $CaCl_2$ and NaOH were purchased from Beijing Chemical Regent Co., Ltd. Bovine serum albumin (BSA) was obtained from Beijing Solarbio Science & Technology Co., Ltd. BCA protein assay kit was purchased from Sigma-Aldrich. All used chemicals were of analytical grade and used directly without further purification. De-ionized water was used throughout the experiments.

2.2. Synthesis of MHA

MHAs were prepared according to the previous literature with some modifications [36]. In a typical process, 5.48 g of $K_2HPO_4 \cdot 3H_2O$ and 8.74 g of cetyltrimethyl-ammonium bromide (CTAB) were dissolved in 100 ml de-ionized water and the solution was adjusted to pH 12 using 1 M NaOH. 4.44 g of $CaCl_2$ was dissolved into 60 ml of de-ionized water. Next, the $CaCl_2$ solution was added dropwise to the solution mixture slowly, yielding a milky suspension, which was refluxed at 120 °C for 24 h. The precipitate was then separated by centrifugation (10,000 rpm, 5 min) and washed several times with ethanol and de-ionized water in turn. A gel-like paste was produced and then dried in an oven at 70 °C for 48 h. The powder was then calcined in a furnace at 500 °C for 6 h to remove CTAB. HA was synthesized without CTAB and refluxed at 120 °C in a similar method with no change in other parameters.

2.3. Characterization

The phase and crystallographic structures of the synthesized MHA and HA were characterized by an X-ray diffraction (XRD) instrument, Bruker D8 ADVANCE diffractometer, with CuKα (target) radiation ($\lambda = 1.54$ Å) with a step size of 0.02° 2θ, and a scan range from $2\theta =$ 20 to 80°. Fourier transform infrared spectroscopy (FTIR) spectra were recorded on a Perkin d Elmer 580B IR spectrophotometer using KBr pellet technique. Nitrogen (N_2) adsorption–desorption isotherms were collected in a Quantachrome Autosorb-1 gas adsorption analyzer at 77 K after degassing the samples at 473 K for 24 h. The surface areas of sample powders were calculated according to the Barrett–Emmett–Teller (BET) equation using the data between 0.05 and 0.35. The relative pressure P/Po of the isotherm was studied between 0.01 and 1.0. The pore parameters were calculated from the desorption branches of the isotherm from the Barrett–Joyner–Halanda model. Transmission electron microscope (TEM) images were used to observe the morphology of

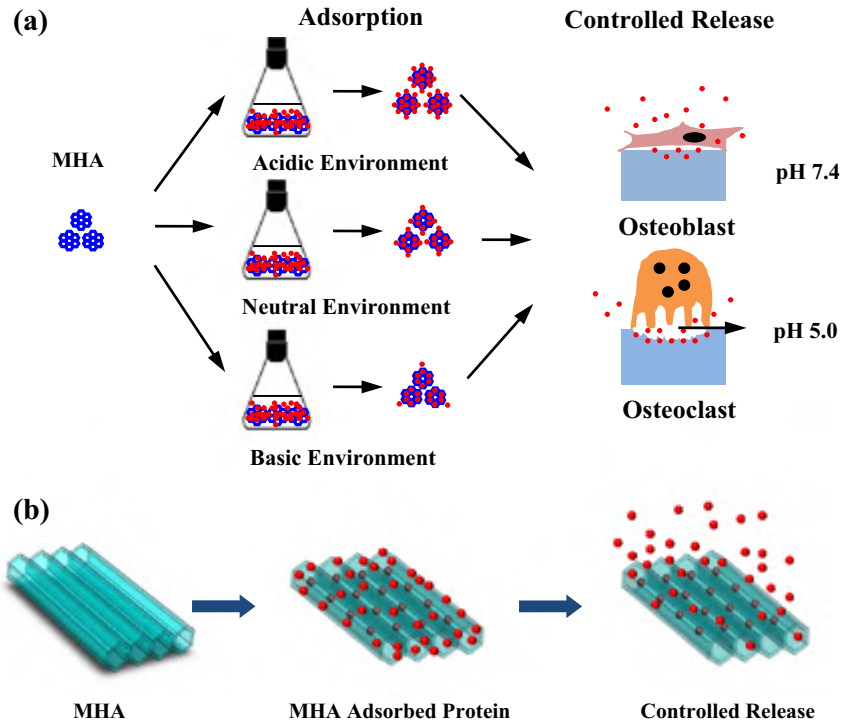

Scheme 1. Schematic illustration of encapsulation and release pathways of proteins within mesopores of MHA under different environmental solution pHs in macro-view (a) and micro-view (b).

powder samples on an FEI Tecnai G2 S-Twin with an acceleration voltage of 200 kV. The TEM specimens were prepared by depositing a drop of a powder dispersion, which was prepared in ethanol by ultrasonication for 20 min, on a carbon-coated copper grid and by drying at room temperature. Morphologies of the particles were observed using a Philips XL30 field Emission Scanning Electron Microscope (SEM). Zeta potential values in different pH solutions were measured using a Malvern Instrument Nano Series ZS Zetasizer.

2.4. BSA adsorption on MHA and HA

Samples of HA and MHA (0.01 g) were pre-equilibrated with 0.9 ml of phosphate buffer solution (pH range 4.7–8.4) in tubes for 1 h at 37 °C. BSA (0.1 ml, 5.0–20.0 mg/ml) was added to the above suspensions. The tubes (in triplicate) were shaken at 160 rpm and 37 °C until equilibrium was reached. Finally, the BSA-loaded particles were separated by centrifugation and then freeze-dried at −70 °C for 48 h. The amounts of BSA loaded in the particles were measured by determining the concentration reduction in the supernatant, which was analyzed by BCA protein assay (wavelength = 562 nm).

2.5. Adsorption of BSA: Langmuir and Freundlich models

In our study, both Langmuir and Freundlich constants were calculated by linear-fitting of adsorbed proteins. The Langmuir model and the Freundlich model have been used to elucidate the protein adsorption behavior onto HA particle surfaces. The Langmuir model assumes monolayer adsorptions where both the maximum protein adsorption onto surfaces and the equilibrium constant for specific adsorption were estimated from the equation below:

$$C/Q = 1/bQm + C/Q. \quad (1)$$

In the equation, C is the BSA concentration, Qm is the monolayer adsorption capacity, and Q is the amount of BSA adsorbed on the adsorbent. Langmuir's equilibrium constant is expressed as b which measures the strength of interaction between protein and particle surface. The Freundlich model is suitable for heterogeneous systems and takes into consideration the multi-layer protein adsorption and interactions on a heterogeneous surface [37]. The Freundlich equation is as follows:

$$\log Q = \log K_f + \log C/n. \quad (2)$$

The C and Q values are as in the Langmuir equation, while n is the Freundlich constant and K_f is the binding-energy constant.

2.6. BSA release from MHA and HA

MHA adsorbed BSA and HA adsorbed BSA were prepared at 2 mg/ml BSA solution under different pHs. The HAs which adsorbed BSA at solutions pH 4.7, pH 7.4 and pH 8.4 were abbreviated as $HA_{pH\ 4.7}$, $HA_{pH\ 7.4}$ and $HA_{pH\ 8.4}$. The MHAs which adsorbed BSA at solutions pH 4.7, pH 7.4 and pH 8.4 were abbreviated as $MHA_{pH\ 4.7}$, $MHA_{pH\ 7.4}$ and $MHA_{pH\ 8.4}$, respectively. All samples for release experiments were incubated in a constant temperature vibrator at 37 °C with a vibrating speed of 60 rpm. The experiment was done in triplicate. At the pre-designed time intervals, 0.1 ml of solution of release medium was taken out from each vial and equal volume of fresh PBS was replenished. The accumulated release of BSA was analyzed by BCA protein assay. The $MHA_{pH\ 7.4}$ and BSA-released $MHA_{pH\ 7.4}$ at pH 7.4 were detected by Nitrogen (N_2) adsorption–desorption.

3. Results and discussion

3.1. Characteristics of HA and MHA

3.1.1. XRD and FTIR analyses

Fig. 1 shows the XRD patterns of HA and MHA and the standard data for the hexagonal hydroxyapatite, respectively. The main observed crystalline peaks of MHA are at diffraction angles of 25.99, 29.10, 31.84, 39.94, and 46.61° with d spacing of 3.43, 3.06, 2.80, 2.25, and 1.94 Å, respectively. In the case of HA, the crystalline peaks were observed at slightly different diffraction angles of 25.49, 31.79, 31.86, 34.09, 39.66, and 46.39° with d spacings of 3.53, 2.81, 2.74, 2.69, 2.29, and 1.96 Å, respectively. No characteristic diffraction angles from other calcium phosphate phases are detected in XRD patterns. These d values of both HA and MHA corresponded to that of hexagonal HA [$Ca_{10}(PO_4)_6(OH)_2$] (JCPDS-International Center for Diffraction Data, card no. 09-0432). The respective calculated lattice constants of a = 0.9417 nm, c = 0.6881 nm and a = 0.9412 nm, c = 0.6879 nm are calculated for HA and MHA respectively. The XRD patterns also revealed that the structure of HA and MHA belongs to the hexagonal P63/m space group with lattice constants of a = 0.9418 nm and c = 0.6884 nm. FTIR spectra of MHA before and after calcination are shown in Fig. 2. IR bands at 3433 cm^{-1} belong to the vibrational mode of structural OH groups of hydroxyapatite (Fig. 2a). Phosphate absorption bands occur at about 1075, 1033, 940, 601 and 562 cm^{-1}, which are all characteristic for a typical hydroxyapatite FTIR spectrum [38]. The strong absorption bands at 2918 and 2849 cm^{-1} are assigned to CH_2 stretching modes of CTAB [18]. After the calcination at 500 °C, the strong bands at 2918 and 2849 cm^{-1} have vanished (Fig. 2b), implying no residual CTAB species in the calcined sample.

3.1.2. SEM and TEM

The SEM and TEM images of the HA and MHA samples are displayed in Figs. 3 and 4, respectively. Both samples consist of relatively uniform rod-like particles with the width of 20–30 nm. But the length of MHA (100–200 nm) is much longer than that of HA (35–45 nm). As shown in Fig. 4, the rod-like morphology of HA or MHA observed with TEM is consistent with the SEM results (Fig. 3). The results indicate that the presence of CTAB has great influence on the morphology of hydroxyapatite particles. The reason may be is that the presence of CTAB micelles in the reaction system benefits hydroxyapatite nucleation and crystal growth. The mesopores of MHA are observed mostly in disordered arrangement in the TEM image, but there are also a few domains where pores are arranged in order (inset circle in Fig. 4d). The TEM image shown in Fig. 4d also reveals light shaded fringes within the rod-like structure. These shaded fringes represent the boundaries of nano-

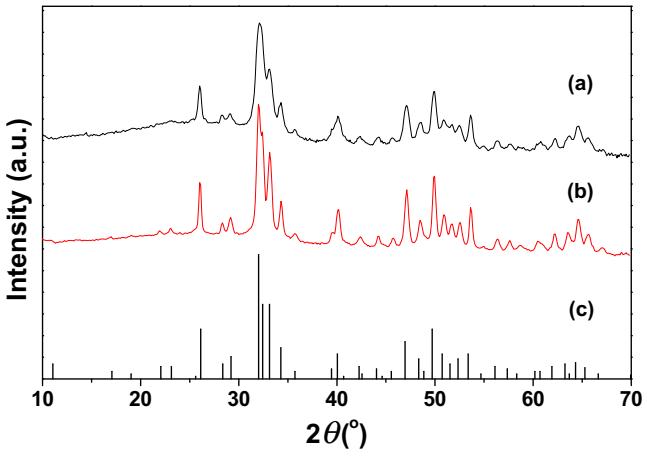

Fig. 1. Wide-angle XRD patterns of HA (a), MHA (b), and the standard data for hydroxyapatite (JCPDS No. 09-0432) (c).

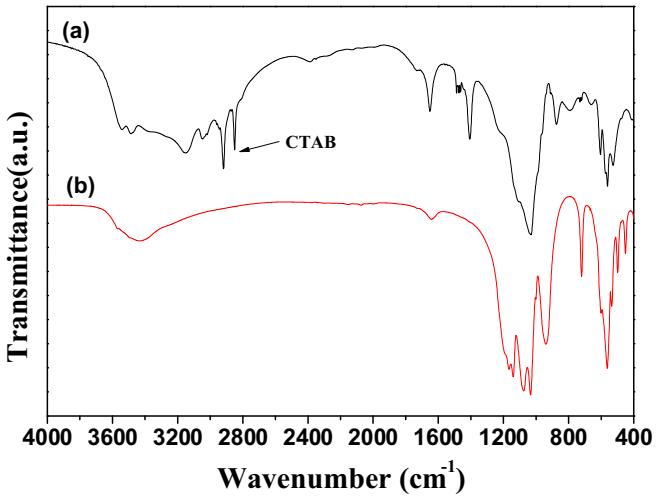

Fig. 2. FTIR spectra of MHA before (a) and after calcination (b).

channels formed. These nano-channels are consistent with the cavities generated by the removal of "organic" CTAB templating structures during calcination. A credible mechanism for the formation of mesoporous structure is that CTAB–PO_4^{3-} mixtures form rod-like micelles, which consist of many PO_4^{3-} species bound to the surface, and after Ca^{2+} is added into the solution, a CTAB–calcium phosphate cluster is formed due to the conformational compatibility between the identical hexagonal shape of the micelle and calcium phosphate. The micelles act as nucleating points for the growth of MHA crystals. The crystals coalesce to form a stable 3D rod-like structure. After that, the MHA powders are obtained by calcining to remove CTAB molecules [18,39].

3.1.3. N_2 adsorption/desorption

The respective N_2 adsorption/desorption isotherms of pure HA and MHA are shown in Fig. 5a and b. It can be seen that all the samples except HA show similar VI isotherms and the typical H1-hysteresis loops, demonstrating the properties of typical mesoporous materials. The textural parameters of the corresponding materials are summarized in Table 1. As shown, the pure MHA has BET surface area (S_{BET}) of 52.29 ± 3.31 m^2/g, pore volume (V_P) of 0.38 ± 0.01 cm^3/g, and average pore size (D_P) of 24.09 ± 2.31 nm, which is much higher than those of HA.

3.2. Protein loading properties

3.2.1. Quantity of protein adsorption depended on time

The protein adsorption onto HA or MHA was evaluated with a model protein (BSA) at phosphate buffered medium. The time–adsorption curve of BSA at pH 7.4 is shown in Fig. 6. As shown in Fig. 6, after soaking in BSA solution for 12 h, the adsorption curves reach plateau phase. The equilibrium capacity was 68.10 ± 1.01 mg/g for MHA and 35.24 ± 2.05 mg/g for HA. The results demonstrated that MHA had a greatly improving protein loading capacity, nearly double that of HA. A number of factors are important in determining the amount of protein adsorbed on surfaces [6,10,16,17,20]. A higher surface area generally corresponds to a higher amount of protein adsorption [10,16]. The specific surface area of MHA exceeds that of HA significantly, thus MHA is expected to exhibit a higher amount of adsorption than HA. As shown in Table 1, for $MHA_{pH\ 7.4}$, the respective S_{BET} (34.60 m^2/g), V_P (0.32 cm^3/g) and D_P (19.45 nm) markedly reduced compared with pure MHA. This is because mesoporous structures of MHA allow proteins to be hosted in nanoscale pores, enhancing the capacity for protein adsorption [10]. For the adsorption isotherm experiments, a time period of 12 h was used.

3.2.2. BSA adsorption on MHA and HA as a function of medium pH

As shown in Fig. 7, BSA adsorption on HA or MHA in PBS of different pHs was evaluated. For BSA adsorption on MHA, adsorption increased as the solution pH decreased from 8.4 to 4.7. MHA had the highest amount of adsorption at each BSA concentration at pH 4.7. BSA adsorption on HA has a very similar trend to MHA. The results suggest that the adsorbed amount of protein on MHA or HA particles depended on pH and concentration of protein solution. The amount of adsorbed protein onto particles was closely correlated with the particles' surface charges [16,22]. Fig. 8 shows that zeta potential values of both particles moved toward negative value by increasing the pH, which agrees with the idea that the number of hydroxide ions surrounding the particles will be higher in an alkaline solution. Our study has also demonstrated that more protein was adsorbed onto the surface of both particles by decreasing the pH of working solution. In our study, the amount of BSA adsorption was negatively correlated with zeta potential values. Repulsive charge forces between particles and BSA molecules disfavor molecular interactions and further adsorption. In addition, the lateral repulsion between the protein molecules is more significant at higher solution pH, which also plays a role in lower adsorption.

3.3. Protein release properties

Fig. 9 shows the cumulative release kinetics of BSA from $HA_{pH\ 7.4}$ and $MHA_{pH\ 7.4}$ at pH 7.4. The release rate of BSA from HA was very rapid. An initial burst in the first hour released 68.65% of adsorbed BSA, and the rate kept almost constant during the next hours. However, for $MHA_{pH\ 7.4}$, a different protein release kinetic was observed, showing a sustained release over 6 h followed by a more gradual release. An initial sustained release in the first 3 h released 49.55% of the protein, but after that BSA release was more gradual. As shown in Fig. 4d, for BSA-released $MHA_{pH\ 7.4}$, the respective S_{BET} (42.09 ± 7.80 m^2/g), V_P (0.35 ± 0.04 cm^3/g) and D_P (22.56 ± 2.42 nm) decreased compared with $MHA_{pH\ 7.4}$, which indicated that BSA was released from mesopores partially. It was deduced that the capillary channels as a mechanical barrier played an important role in BSA sustained release from MHA.

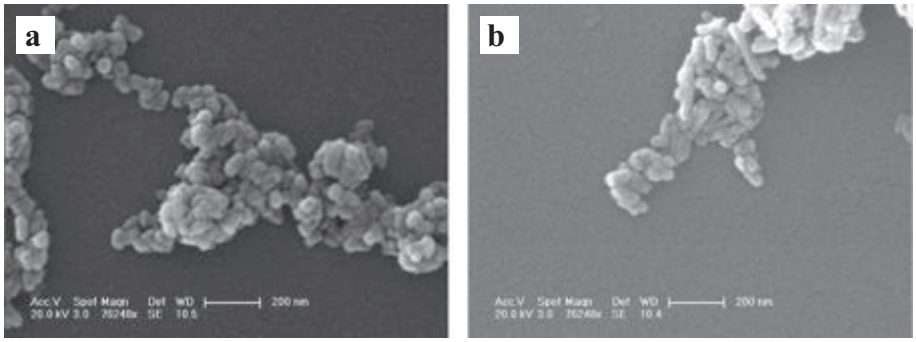

Fig. 3. SEM images of HA (a) and MHA (b).

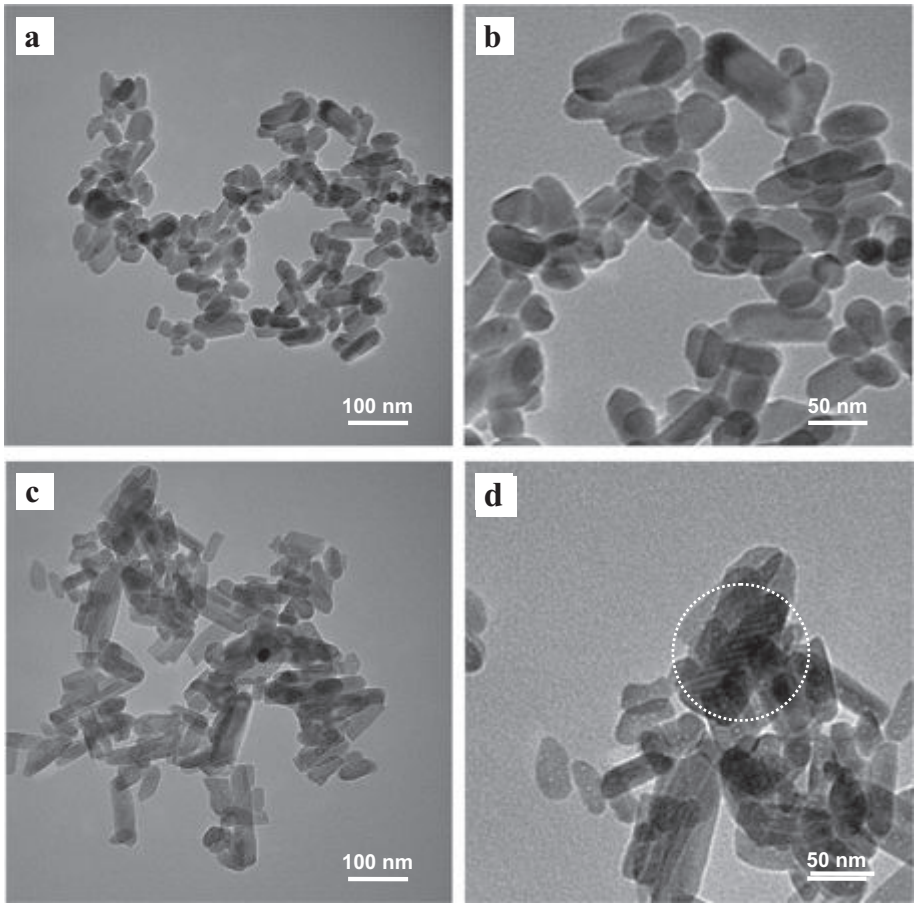

Fig. 4. TEM images of HA (a and b) and MHA (c and d).

Our data are in good agreement with the earlier observations for mesoporous calcium silicates [10].

Fig. 10a and b shows the cumulative release kinetics of BSA from $MHA_{pH\ 4.7}$, $MHA_{pH\ 7.4}$ and $MHA_{pH\ 8.4}$ immersed in neutral (pH 7.4) and acidic (pH 5.0) environment, respectively. $MHA_{pH\ 4.7}$, $MHA_{pH\ 7.4}$ and $MHA_{pH\ 8.4}$ reached to a gradual release after a sustained release for 2 h, 2 h and 4 h at pH 7.4, but for 3 h, 4 h and 6 h at pH 5.0, respectively. Among them, $MHA_{pH\ 8.4}$ showed a more sustained release curve compared with $MHA_{pH\ 4.7}$ and $MHA_{pH\ 7.4}$ whether in acidic or neutral environment, indicating that the release of protein from MHA particles could be regulated by its environment pH of protein adsorption. Furthermore, $MHA_{pH\ 8.4}$ showed 2 h longer of sustained release in acidic environment than that in neutral environment, indicating its specific application in drug delivery.

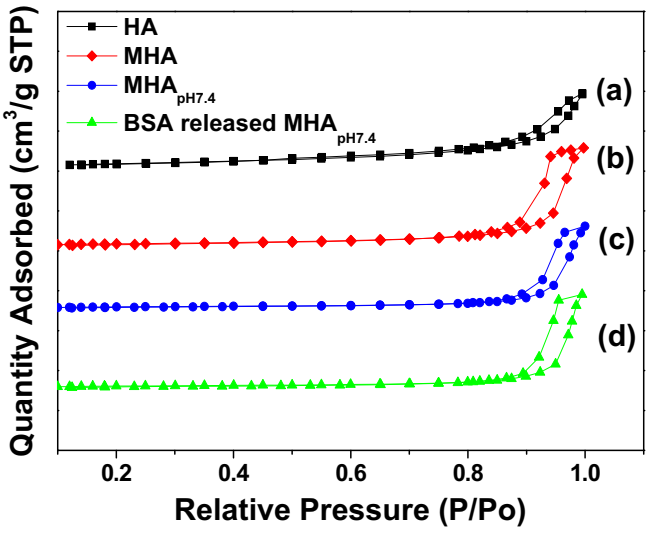

Fig. 5. N_2 adsorption/desorption isotherms for HA (a), MHA (b), $MHA_{pH\ 7.4}$ (c) and BSA released $MHA_{pH\ 7.4}$ (d).

3.4. Langmuir and Freundlich models for BSA adsorption and release on MHA

Table 2 summarizes regression coefficient (r^2) for Langmuir isotherm. Given that the correlation coefficient for this model ranged from 0.9067 to 0.9972 over different buffer pHs, the Langmuir model predictions are well correlated with the experimental data. MHA had the higher binding capacity (4.0025 mg/m^2) than HA (2.8932 mg/m^2), which was calculated using Eq. (1). As an increase of pH value, the strength of interaction between protein and particle surface (b value) decreased, corresponding to the change of Qm value.

In general, the correlations obtained with the Freundlich model for different pHs were closer to 1 than those obtained with the Langmuir model. The 1/n values from the Freundlich model are generally higher

Table 1
Textural parameters of HA, MHA, $MHA_{pH\ 4.7}$ and BSA released $MHA_{pH\ 4.7}$ samples.

Samples	V_p (cm^3/g)	S_{BET} (m^2/g)	D_p (nm)
HA	0.23 ± 0.01	30.66 ± 4.00	14.55 ± 1.79
MHA	0.38 ± 0.01	52.29 ± 3.31	24.09 ± 2.31
$MHA_{pH\ 4.7}$	0.32 ± 0.03	34.60 ± 2.45	19.45 ± 0.46
BSA released $MHA_{pH\ 4.7}$	0.35 ± 0.04	42.09 ± 7.80	22.56 ± 2.42

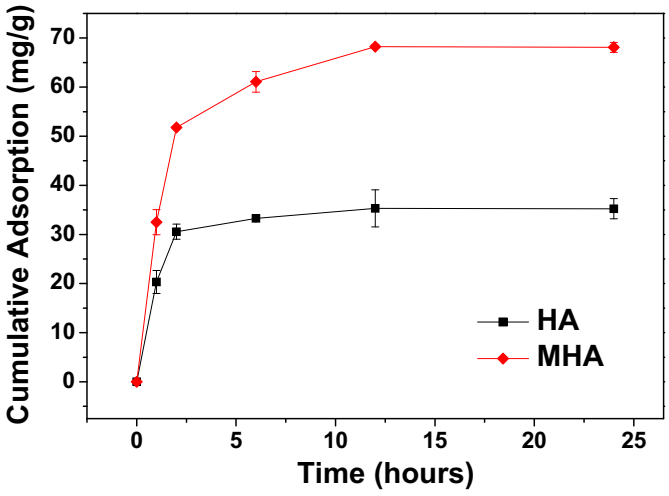

Fig. 6. The kinetics of proteins adsorption on HA and MHA in 1.5 mg/ml BSA solution at pH 7.4.

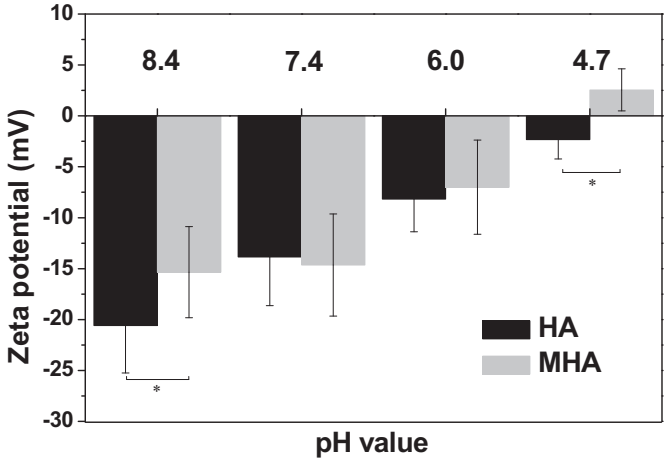

Fig. 8. The changes in zeta potential values of HA and MHA as function of pH of working solution (*$p < 0.05$, n = 30).

for the samples with a higher protein-loading capacity. For example, the BSA adsorptions onto MHA at pH 4.7 and pH 6.0 showed higher 1/n value (0.6181 and 0.6926, respectively) compared with those at pH 7.4 and pH 8.4 (0.4625 and 0.4952, respectively). This is in agreement with the high amount of BSA adsorption on the samples in general.

Lee et al. concluded in their study that BSA and lysozyme adsorption onto amino acid-functionalized hydroxyapatite particles fitted better with the model Freundlich than the Langmuir model [22]. However, based on our results, Freundlich model showed a similar efficacy in predicting the adsorption of proteins onto the surfaces of MHA as demonstrated in similar r^2 values when compared with the Langmuir model. This suggests that the protein adsorption over MHA tends to be a mono-layer adsorption. Both the Langmuir and Freundlich models should be used to predict the adsorption of proteins. The heterogeneity index, 1/n, varies from close to zero for a very heterogeneous surface to one for a homogeneous surface. The calculated 1/n for BSA adsorption onto MHA is 0.848 (Table 2), which shows a relatively high degree of homogeneity.

The change of the *b* value in the Langmuir equation at different pH values provided a logical explanation for protein release properties, as *b* measures the strength of interaction between the protein and particle surface. A decrease of pH results in a decrease of the *b* value. As $MHA_{pH\ 8.4}$ is transferred to an acidic environment, the strength of interactions increases and the adsorption equilibrium of BSA to MHA shifts toward the unsaturated state. The strength of interactions between protein and particle surface should be enough to prevent

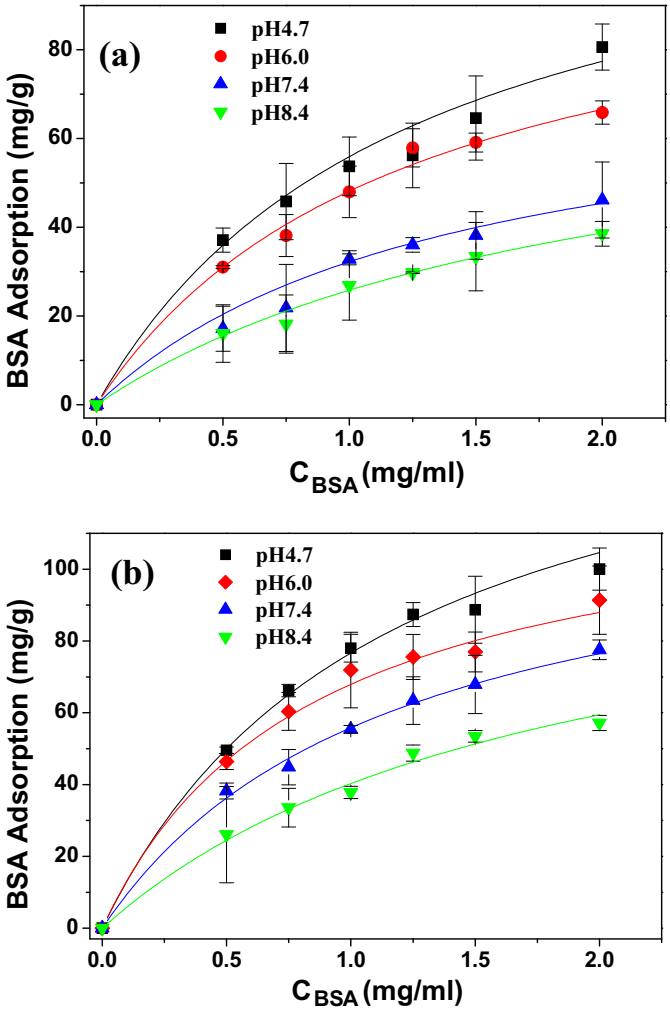

Fig. 7. Adsorption isotherms of BSA over HA (a) or MHA (b) in different pHs of working solution (pH 4.7, 6.0, 7.4 and 8.4).

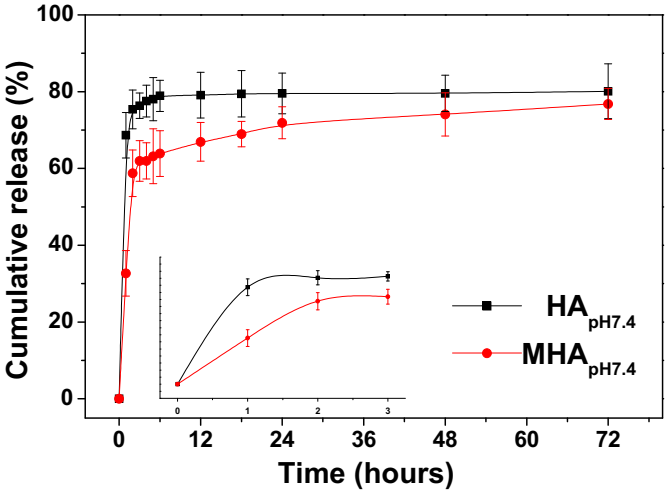

Fig. 9. The cumulative release kinetics of BSA from $HA_{pH\ 7.4}$ and $MHA_{pH\ 7.4}$ (n = 3).

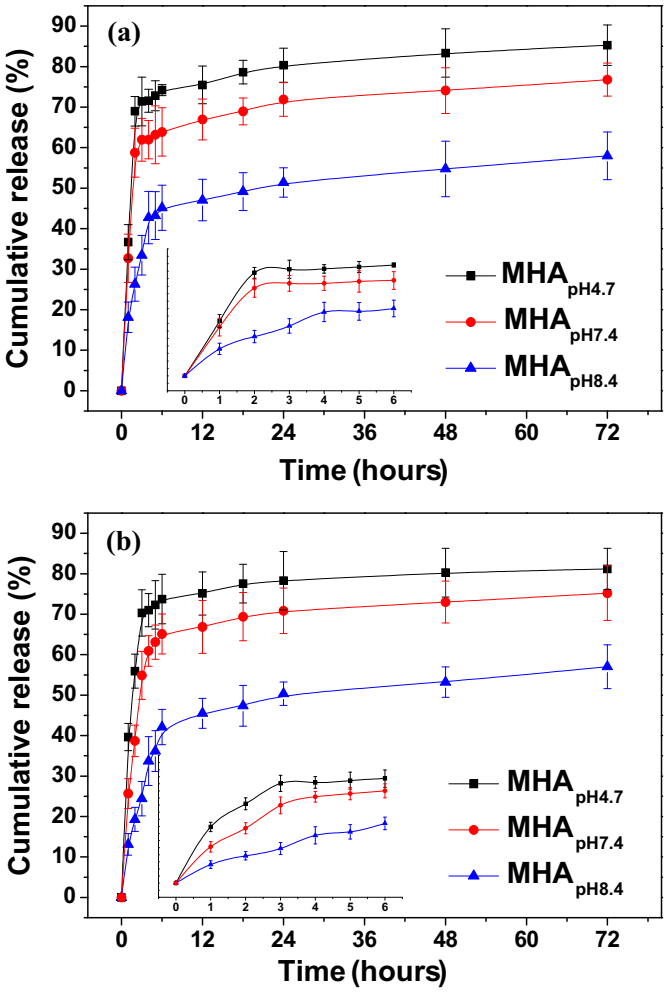

Fig. 10. Release profiles from $MHA_{pH\ 4.7}$, $MHA_{pH\ 7.4}$ and $MHA_{pH\ 8.4}$ at pH 7.4 (a) and pH 5.0 (b), respectively (n = 3).

BSA bursting release from MHA. Accordingly, MHA adsorbed BSA in a basic environment exhibited a more controlled release in acidic environments, and cumulative release was relatively lower among all samples in acidic environments. On the contrary, for MHA adsorbed BSA in acidic environments and subsequently transferred to a neutral environment, the cumulative release became much higher as *b* value decreased.

MHA has been regarded as a perfect candidate for both bone repair and drug delivery, so our findings may be very useful for the development of these applications. For instance, an isolated acid microenvironment can be established by the osteoclast between itself and bone [30], where local pH around the ruffled border of osteoclasts is from 4.0 to 5.0 [31,32]. The MHA adsorbed OPG in specific pH environments exhibits a sustained release pattern in this acid environment (Scheme 2). The activation of RANK would be prevented by OPG binding to RANKL and OPG can also induce apoptosis of osteoclast [33–35].

Table 2
Langmuir and Freundlich parameters for BSA adsorption over MHA.

pH	Langmuir parameters			Freundlich parameters		
	r^2	Qm (mg/m^2)	*b* (l/mg)	r^2	1/n	K_f
4.7	0.9972	4.0025	1.2177	0.9756	0.6181	0.9756
6.0	0.9854	3.3408	1.1922	0.9467	0.6926	0.9467
7.4	0.9668	2.7775	1.0481	0.9728	0.4625	0.9728
8.4	0.9067	2.6098	0.6891	0.9235	0.4951	0.9235

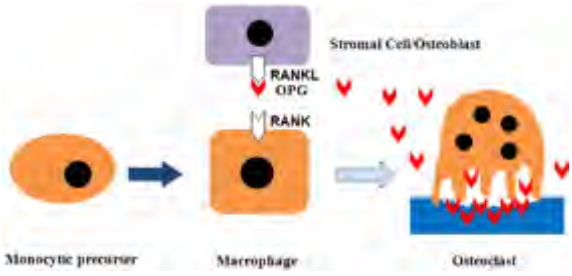

Scheme 2. Schematic illustration of the regulation of osteoclast maturation and activation negatively by controlled released of OPG in acidic environment.

4. Conclusions

MHA as a bioactive protein delivery system has been synthesized in this work and its loading and release of protein influenced by environmental pH were studied. The results show that the loading amounts of BSA on MHA decreased as the pH increased, indicating they greatly depended on environmental pH. Furthermore, the release behavior could be regulated by environmental pH of protein adsorption. Among them, $MHA_{pH\ 8.4}$ exhibited a more sustained release kinetics compared with $MHA_{pH\ 4.7}$ and $MHA_{pH\ 7.4}$, and especially its release in acidic environment was sustained longer than that in neutral environment. It elicits a potential application in targeted delivery of drugs for the therapy of bone defects or bone diseases, such as specific delivery of drugs in the acidic environment established by osteoclasts.

Acknowledgments

The authors gratefully acknowledge the financial support from the National Natural Science Foundation of China (nos. 51273081, 51103149 and no. 51273195), the Project of International Cooperation from the Ministry of Science and Technology of the People's Republic of China (no. S2013GR04340), the Major Project of Science and Technology of Jilin Province (20130201005GX), and the Science and Technology Foundation of Changchun (no. 2012092).

References

[1] K.E. Uhrich, S.M. Cannizzaro, R.S. Langer, K.M. Shakesheff, Polymeric systems for controlled drug release, Chem. Rev. 99 (1999) 3181–3198.
[2] L. Di Silvio, W. Bonfield, Biodegradable drug delivery system for the treatment of bone infection and repair, J. Mater. Sci. Mater. Med. 10 (1999) 653–658.
[3] E. Esposito, R. Cortesi, C. Nastruzzi, Gelatin microspheres: influence of preparation parameters and thermal treatment on chemico-physical and biopharmaceutical properties, Biomaterials 17 (1996) 2009–2020.
[4] Y.J. Xia, P.F. Ribeiro, D.W. Pack, Controlled protein release from monodisperse biodegradable double-wall microspheres of controllable shell thickness, J. Control. Release 172 (2013) 707–714.
[5] S.E. Bae, J. Choi, Y.K. Joung, K. Park, D.K. Han, Controlled release of bone morphogenetic protein (BMP)-2 from nanocomplex incorporated on hydroxyapatite-formed titanium surface, J. Control. Release 160 (2012) 676–684.
[6] T. Matsumoto, M. Okazaki, M. Inoue, S. Yamaguchi, T. Kusunose, T. Toyonaga, et al., Hydroxyapatite particles as a controlled release carrier of protein, Biomaterials 25 (2004) 3807–3812.
[7] D.M. Arm, A.F. Tencer, S.D. Bain, D. Celino, Effect of controlled release of platelet-derived growth factor from a porous hydroxyapatite implant on bone ingrowth, Biomaterials 17 (1996) 703–709.
[8] Y.J. Guo, Y.Y. Wang, T. Chen, Y.T. Wei, L.F. Chu, Y.P. Guo, Hollow carbonated hydroxyapatite microspheres with mesoporous structure: hydrothermal fabrication and drug delivery property, Mater. Sci. Eng. C Mater. Biol. Applic. 33 (2013) 3166–3172.
[9] I.I. Slowing, B.G. Trewyn, S. Giri, V.S.Y. Lin, Mesoporous silica nanoparticles for drug delivery and biosensing applications, Adv. Funct. Mater. 17 (2007) 1225–1236.
[10] W. Xue, A. Bandyopadhyay, S. Bose, Mesoporous calcium silicate for controlled release of bovine serum albumin protein, Acta Biomater. 5 (2009) 1686–1696.
[11] M.A. Rauschmann, T.A. Wichelhaus, V. Stirnal, E. Dingeldein, L. Zichner, R. Schnettler, et al., Nanocrystalline hydroxyapatite and calcium sulphate as biodegradable composite carrier material for local delivery of antibiotics in bone infections, Biomaterials 26 (2005) 2677–2684.
[12] C. Wu, Y. Ramaswamy, Y. Zhu, R. Zheng, R. Appleyard, A. Howard, et al., The effect of mesoporous bioactive glass on the physiochemical, biological and drug-release properties of poly(DL-lactide-co-glycolide) films, Biomaterials 30 (2009) 2199–2208.

[13] Y.J. Guo, T. Long, W. Chen, C.Q. Ning, Z.A. Zhu, Y.P. Guo, Bactericidal property and biocompatibility of gentamicin-loaded mesoporous carbonated hydroxyapatite microspheres, Mater. Sci. Eng. C Mater. Biol. Applic. 33 (2013) 3583–3591.
[14] J.E. Barralet, K.J. Lilley, L.M. Grover, D.F. Farrar, C. Ansell, U. Gbureck, Cements from nanocrystalline hydroxyapatite, J. Mater. Sci. Mater. Med. 15 (2004) 407–411.
[15] A. Almirall, G. Larrecq, J.A. Delgado, S. Martinez, J.A. Planell, M.P. Ginebra, Fabrication of low temperature macroporous hydroxyapatite scaffolds by foaming and hydrolysis of an alpha-TCP paste, Biomaterials 25 (2004) 3671–3680.
[16] W.H. Lee, C.Y. Loo, A.V. Zavgorodniy, R. Rohanizadeh, High protein adsorptive capacity of amino acid-functionalized hydroxyapatite, J. Biomed. Mater. Res. A 101A (2013) 873–883.
[17] M. Mohsen-Nia, M.M. Bidgoli, M. Behrashi, A.M. Nia, Human serum protein adsorption onto synthesis nano-hydroxyapatite, Protein J. 31 (2012) 150–157.
[18] N. Pramanik, T. Imae, Fabrication and characterization of dendrimer-functionalized mesoporous hydroxyapatite, Langmuir 28 (2012) 14018–14027.
[19] C.K. Poh, S. Ng, T.Y. Lim, H.C. Tan, J. Loo, W. Wang, In vitro characterizations of mesoporous hydroxyapatite as a controlled release delivery device for VEGF in orthopedic applications, J. Biomed. Mater. Res. A 100 (2012) 3143–3150.
[20] S. Ng, J. Guo, J. Ma, S.C. Loo, Synthesis of high surface area mesostructured calcium phosphate particles, Acta Biomater. 6 (2010) 3772–3781.
[21] Y. Zhang, N. Cheng, R. Miron, B. Shi, X. Cheng, Delivery of PDGF-B and BMP-7 by mesoporous bioglass/silk fibrin scaffolds for the repair of osteoporotic defects, Biomaterials 33 (2012) 6698–6708.
[22] W.H. Lee, C.Y. Loo, K.L. Van, A.V. Zavgorodniy, R. Rohanizadeh, Modulating protein adsorption onto hydroxyapatite particles using different amino acid treatments, J. R. Soc. Interface 9 (2012) 918–927.
[23] D.T. Wassell, R.C. Hall, G. Embery, Adsorption of bovine serum albumin onto hydroxyapatite, Biomaterials 16 (1995) 697–702.
[24] S.M. Lim, S.H. Oh, H.H. Lee, S.H. Yuk, G.I. Im, J.H. Lee, Dual growth factor-releasing nanoparticle/hydrogel system for cartilage tissue engineering, J. Mater. Sci. Mater. Med. 21 (2010) 2593–2600.
[25] Y. Bai, P.P. Li, G.F. Yin, Z.B. Huang, X.M. Liao, X.C. Chen, et al., BMP-2, VEGF and bFGF synergistically promote the osteogenic differentiation of rat bone marrow-derived mesenchymal stem cells, Biotechnol. Lett. 35 (2013) 301–308.
[26] C.L. Ferreira, F.A.M. de Abreu, G.A.B. Silva, F.F. Silveira, L.B.A. Barreto, T.D. Paulino, et al., TGF-beta 1 and BMP-4 carried by liposomes enhance the healing process in alveolar bone, Arch. Oral Biol. 58 (2013) 646–656.
[27] M. Kaipel, S. Schutzenberger, A. Schultz, J. Ferguson, P. Slezak, T.J. Morton, et al., BMP-2 but not VEGF or PDGF in fibrin matrix supports bone healing in a delayed-union rat model, J. Orthop. Res. 30 (2012) 1563–1569.
[28] A.P. White, A.R. Vaccaro, J.A. Hall, P.G. Whang, B.C. Friel, M.D. McKee, Clinical applications of BMP-7/OP-1 in fractures, nonunions and spinal fusion, Int. Orthop. 31 (2007) 735–741.
[29] C. Yang, W. Guo, L. Cui, D. Xiang, K. Cai, H. Lin, et al., pH-responsive controlled-release system based on mesoporous bioglass materials capped with mineralized hydroxyapatite, Mater. Sci. Eng. C Mater. Biol. Applic. 36 (2014) 237–243.
[30] S.L. Teitelbaum, Bone resorption by osteoclasts, Science 289 (2000) 1504–1508.
[31] Paul H. Schlesinger, H.C. Blair, Steven L. Teitelbaum, John C. Edwards, Characterization of the osteoclast ruffled border chloride channel and its role in bone resorption, J. Biol. Chem. 272 (1997) 18636–18643.
[32] R.N.L. Baron, D. Louvard, P.J. Courtoy, Cell-mediated extracellular acidification and bone resolution, J. Cell Biol. 101 (1985) 2210–2222.
[33] W.S. Simonet, D.L. Lacey, C.R. Dunstan, M. Kelley, M.S. Chang, R. Luthy, et al., Osteoprotegerin: a novel secreted protein involved in the regulation of bone density, Cell 89 (1997) 309–319.
[34] D. Aeschlimann, B.A. Evans, The vital osteoclast: how is it regulated? Cell Death Differ. 11 (Suppl. 1) (2004) S5–S7.
[35] Y.X. Fu, J.H. Gu, Y.R. Zhang, X.S. Tong, H.Y. Zhao, Y. Yuan, et al., Influence of osteoprotegerin on differentiation, activation, and apoptosis of Gaoyou duck embryo osteoclasts in vitro, Poult. Sci. 92 (2013) 1613–1620.
[36] J. Yao, W. Tjandra, Y.Z. Chen, K.C. Tam, J. Ma, B. Soh, Hydroxyapatite nanostructure material derived using cationic surfactant as a template, J. Mater. Chem. 13 (2003) 3053.
[37] M. Iafisco, B. Palazzo, G. Falini, M.D. Foggia, S. Bonora, S. Nicolis, et al., Adsorption and conformational change of myoglobin on biomimetic hydroxyapatite nanocrystals functionalized with alendronate, Langmuir 24 (2008) 4924–4930.
[38] P. Yang, Z. Quan, C. Li, X. Kang, H. Lian, J. Lin, Bioactive, luminescent and mesoporous europium-doped hydroxyapatite as a drug carrier, Biomaterials 29 (2008) 4341–4347.
[39] J. Yao, W. Tjandra, Y.Z. Chen, K.C. Tam, J. Ma, B. Soh, Hydroxyapatite nanostructure material derived using cationic surfactant as a template, J. Mater. Chem. 13 (2003) 3053–3057.